Ecosystems (2026)29:41
https://doi.org/10.1007/s10021-026-01064-0

ECOSYSTEMS

ORIGINAL ARTICLE

Long-Term Vegetation Changes Across the Canadian Forest-Tundra Ecotone Using Historic Air Photos and Satellite Time-Series

H. Travers-Smith,[1]* N. C. Coops,[1] M. A. Wulder,[2] T. C. Lantz,[3] and D. D. Ignace[4]

[1]*Department of Forest Resource Management, University of British Columbia, Vancouver, British Columbia V6T 1Z4, Canada;* [2]*Canadian Forest Service, Pacific Forestry Centre, Natural Resources Canada, Victoria, British Columbia V8Z 1M5, Canada;* [3]*School of Environmental Studies, University of Victoria, Victoria, British Columbia V8W 2Y2, Canada;* [4]*Department of Forest Resources, University of Minnesota, St. Paul, Minnesota 55108, USA*

Abstract

Climate change is shifting the structure and composition of vegetation across the northern forest-tundra ecotone. Multi-spectral satellite images are frequently used to model vegetation dynamics at landscape to continental scales. However, validating these models over large areas remains challenging. As a result, analyses conducted at fine spatial scales are needed to interpret changes derived from medium-resolution satellite imagery. In this research, we used high-resolution air photographs ($n = 27$) captured in the 1930's and 1970's paired with contemporary satellite images from the 2020's to map forest and shrub expansion across four transects crossing the northern treeline in Northwest Territories, Canada. We used these data to compare the likelihood of forest and shrub expansion in relation to distance to the forest limit, climate and fire history. We found that shrub and forest expansion was greater in close proximity to, or above the forest limit at three of the four transects. Forest advance was most limited at our northernmost transect, which was drier, contained white spruce (*Picea glauca*) woodlands, and had steeper topographic gradients. Vegetation dynamics at the southern sites were driven by large fires and recovery within closed black spruce (*Picea mariana*) forests. To better understand how well multi-spectral satellite indices can capture these dynamics, we then compared photo-interpreted change to a classification of vegetation change using Landsat time-series from 1985 to 2021, providing a direct link between two widely used change detection methods with different spatial scales and characteristics. Agreement between datasets varied by vegetation type and transect. Correlation was higher for increases in forest cover vs shrub cover and when using the 1970's historical photos vs the 1930's photos. These results suggest that vegetation change occurring between the 1930's and 1970's decreased correlation with the satellite record

Received 4 September 2025; accepted 31 March 2026

Supplementary Information: The online version contains supplementary material available at https://doi.org/10.1007/s10021-026-01064-0.

Author Contributions H. Travers-Smith was involved in conceptualization, formal analysis, investigation, methodology, visualization and writing—original draft. N.C. Coops contributed to conceptualization, funding acquisition, supervision and writing—review and editing. M.A. Wulder, T.C. Lantz and D.D. Ignace were involved in supervision and writing—review and editing.

Corresponding author; e-mail: hana.traverssmith@ubc.ca

Published online: 30 April 2026

beginning in 1985. These findings provide a multi-site comparison of long-term vegetation dynamics across the Canadian forest-tundra ecotone and highlight the use of historic aerial photographs to corroborate medium-spatial-resolution satellite time-series.

Key words: Landsat; Shrubification; Boreal; Treeline.

Introduction

The forest-tundra ecotone is the transition zone between the boreal forest and the tundra, covering 1.4 million km^2 globally (Brandt, 2009; Payette and others, 2001). Vegetation in the ''treeline'' ecotone is responding to rapid shifts in climate (Frost and others, 2025), with significant implications for future carbon storage (Mekonnen and others, 2018), habitat availability (Rickbeil and others, 2018) and fire regimes (Baltzer and others, 2021; Foster and others, 2022). To date, a variety of remote sensing approaches have been used to map and monitor vegetation change across circumpolar Arctic (Beamish and others, 2020). Satellite imagery shows that the northern edge of the forest-tundra ecotone is undergoing spectral greening, indicating possible northward advance of the boreal biome (Berner & Goetz, 2021; Dial and others, 2024; Feng and others, 2025). However, increases in forest area above the treeline may be outpaced by losses from fires below the treeline (Rotbarth and others, 2023). At the regional scale, analysis of air photos and high-spatial-resolution imagery show a variety of local responses to climate (Frost & Epstein, 2014; Terskaia and others, 2020). In northwestern Canada, the range of upright deciduous shrubs are generally expanding northward, replacing graminoid and herbaceous tundra (Fraser and others, 2014; Moffat and others, 2016), while treelines have shown both advance (Danby & Hik, 2009) and stability (Timoney & Mamet, 2020). Taken together, these analyses indicate that the magnitude and drivers of vegetation change are variable and regionally specific.

Given the variety of methods, data sources, image types, spatial resolution and temporal representation across studies it is challenging to compare results. Multi-spectral satellite imagery from platforms like Landsat and MODIS has been used to model a variety of vegetation attributes, including biomass, canopy height and cover of vegetation functional types (Beck & Goetz, 2011; Berner & Goetz, 2021; Montesano and others, 2009). However, validating these models over large areas remains difficult, and factors unrelated to vegetation, including sub-pixel snow and water, can confound spectral trends (Cunliffe and others, 2020; Hoad and others, 2025; Loranty and others, 2018). Differences in the time-period analyzed also introduce discrepancies in the magnitude and direction of change across different studies, with many satellite-based archives spanning one to four decades (Wulder and others, 2022). Subtle changes in vegetation over these time scales can be difficult to capture with contemporary satellite imagery due to slow reproduction and plant growth at high latitudes (Beamish and others, 2020; Dial and others, 2022). For example, Timoney and others (2020) estimate that it could take up to 70 years for northern spruce stems to establish and become visible on very high-resolution imagery. For an alpine site in the Yukon, Danby & Hik (2009) estimate that it could take 20–30 years.

Historic air photos can be used to map vegetation and land cover change predating the satellite record. When paired with contemporary imagery from aerial photographs or high-spatial-resolution satellites, photo-interpreted change can also be integrated with multi-spectral satellite data (Maher and others, 2021; Timoney & Mamet, 2020). In Canada, the National Air Photo Library (NAPL) holds over 6 million aerial images acquired between 1920 and the present day (Natural Resources Canada, 2011). Photos at different spatial scales and time periods have been used to map vegetation change across the Canadian forest-tundra ecotone (Danby & Hik, 2009; Moffat and others, 2016; Timoney and others, 1992; Timoney, 2023; Timoney & Mamet, 2020; Travers-Smith & Lantz, 2020). Interpreters use variation in color, shape and texture of features to differentiate land cover types and in some cases map the density and size of individual tree stems (Brodie and others, 2019; Danby & Hik, 2009; Lantz and others, 2019). These data have been used to map the boundary of the forest-tundra transition across western Canada (Timoney, 1992), local changes in tree height and density at the treeline (Danby & Hik, 2009) and compare advance of northern tree and shrub lines (Lantz and others, 2019; Travers-Smith & Lantz, 2020). Although the cost, time and logistical requirements of collecting air photos across northern Canada challenge repeated monitoring, they can map fine spatial detail and validate changes observed from the satellite record.

In this research we used historic aerial photographs to 1) map change in forest and shrub expansion across multiple treeline sites and 2) improve interpretation of satellite spectral time-series. First, we paired historic air photos from the 1930's and 1970's with very high-resolution satellite imagery (0.4 m) acquired in the 2020's. Photos were acquired at 1:12,000–1:20,000 scale, for four latitudinal transects across northwestern and central Northwest Territories, Canada. Following established practices of the National Air Photo Library (NAPL), the air photos were digitized to an effective pixel size of 0.2–0.3 m. We grouped photos by site and time-period and compared patterns in forest and shrub expansion across sites. Next, we compared change in forest and shrub cover interpreted using historic air photos with a classification of structural change in vegetation derived from Landsat time-series. The satellite time-series used Landsat imagery from 1985 to 2021 and spaceborne lidar data to model expansion of tall-stature forest (> 3 m) and low-stature shrub (< 3 m) vegetation specifically within the Canadian forest-tundra ecotone (Travers-Smith and others, 2025). These comparisons were used to test the agreement between change detection methods (photo interpretation vs Landsat change classification) across treeline sites and time periods.

Methods

Study Area

We analyzed four air photo transects of varying lengths crossing the northern limit of continuous forest in the NWT, Canada (Figure 1). All our transects were located in the Taiga Shield ecozone and were spaced 200–400 km apart (Ecosystem Classification Group, 2008). Climate across this region is characterized by short summers (June–August) with mean temperatures between 9°C and 14°C (Table 1). Average winter (January–March) temperatures vary between -26°C and -20°C. Data from three long-term monitoring stations within the study area (Figure 1) indicate overall warming between 1970 and 2020, with stronger increases in winter temperatures compared to summer (Table 1). Overall, the two southernmost stations (Yellowknife and Fort Reliance) received more annual precipitation than the northernmost station in Kugluktuk. Trends in precipitation are variable, showing wetting trends in the south and drying trends in northwest, respectively (Table 1).

Transect 1 is the coldest, driest and northernmost site located within the Coppermine Upland (High Subarctic) ecoregion. The Coppermine site hosts open stands of white spruce and an abrupt transition to treeless tundra above the forest limit. Upland bedrock areas are composed of lichens, heath and shrub communities. The Coppermine River flows adjacent to the transect, and more dense spruce and shrub woodlands are present within the river valley. Transect 2 is located in the Great Slave Upland (Low Subarctic) ecoregion at intermediate latitude (Ecosystem Classification Group, 2008). Woodlands in the Great Slave Upland (GSU) are mainly composed of black spruce (*Picea mariana*) and paper birch (*Betula papyrifera*). Low-intensity fires are common in the westernmost portion of this transect, with fires in 1976, 1977 and 1994 (Figure 1). The southernmost transects Transect 3 (Whitefish West) and Transect 4 (Whitefish East) are both located within the Whitefish Plain (High Subarctic) ecoregion. The sites have low relief and host dense stands of black spruce woodlands in the south. The transition to tundra vegetation is more diffuse with pockets of spruce woodlands present across the entire transect. Treeless tundra sites in this region are composed of shrub and lichen communities. The southernmost portion of Transect 4 (Whitefish East) experienced wildfires in 1994, 1997 and 1998, and most of Transect 3 (Whitefish West) is within a recent 2014 fire scar (Figure 1).

Overview of Data Analysis

We acquired panchromatic air photographs ($n = 27$) at scales of 1:12,000 to 1:20,000 from the NAPL across the four study sites (Figure 1). Photos at two transects (T1 and T4) were captured in the 1970's, and photos at the remaining sites (T2 and T3) were from the 1930's. First, we used the air photos to assess the historic percent cover of forest, shrub and herbaceous vegetation within 300 × 300 m grid cells ($n = 2{,}063$) encompassing the entire extent of the air photos. To map change in forest and shrub cover we compared historic air photographs to pansharpened World View-2 and 3 images from 2022 and 2024 at a level of spatial detail similar to the digitized air photos (0.4–0.5 m). We used these data to model the probability of increasing forest and shrub cover as a function of distance to the northern forest limit. In the second stage of analysis, we used the photo interpretation to validate changes in vegetation structure classified using Landsat time-series from 1985 to 2021. Vegetation change was classified as

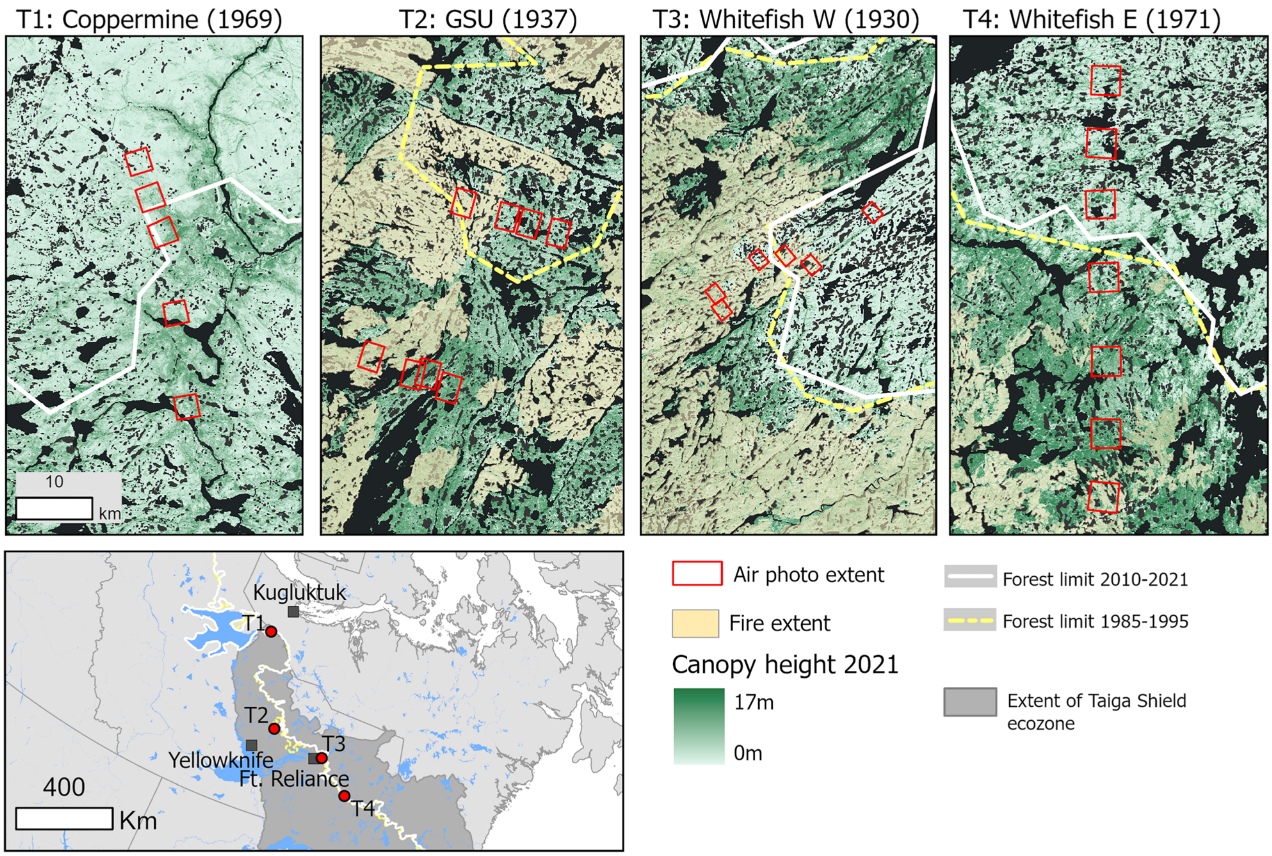

Figure 1. Study area maps (top) showing the extent of historic air photos and modeled canopy height across four transects in the Northwest Territories, Canada representing the transition from forest to tundra land cover. The bottom map shows the location of each transect (red circles) relative to the forest limit (white line). The gray squares indicate long-term weather stations close to the study sites.

Table 1. Summary of Climate Normals for Three Long-Term Monitoring Stations Within Our Study Area

	Mean summer temp (°C)	Mean winter temp (°C)	Total annual precipitation (mm)	Degree days > 5°
Kugluktuk				
1971–2000	8.2	− 26.8	249	387
1991–2020	8.9	− 26.0	233	440
Yellowknife				
1971–2000	14.8	− 22.5	280	1077
1991–2020	15.1	− 21.6	293	1108
Fort Reliance				
1971–2000	12.4	− 25.0	271	815
1991–2020	13.5	− 23.2	–	–

Climate normals are from the 1971–2000 and 1991–2020 periods. Data are publicly available and compiled by Climate Change & Environment Canada (https://climate.weather.gc.ca/climate_normals/index_e.html). Summer temperatures are calculated for June–August, and winter temperatures are January–March. Note data for the 1991–2020 period are not yet available at Fort Reliance.

stable, decreasing or increasing for either forest or tall shrub vegetation. This classification is based on models of canopy height trained using spaceborne lidar data from ICESat-2, with methods fully described in Travers-Smith and others, (2024, 2025).

Data

Historic Air Photos

We assessed the suitability of ∼ 16,000 photos from the National Air Photo Library using photo locations and metadata and identified four areas with historic imagery that crossed the historic (1985–1995) limit of continuous forest (Travers-Smith and others, 2025). Photo selection was opportunistic based on availability, image quality and cost and is not necessarily representative of the entire study area. Photos were considered for selection if they met the following criteria: (1) were within 50 km of the forest limit mapped in Travers-Smith and others (2025), (2) were acquired at 1:20,000 scale or finer, (3) were snow and ice free, (4) and were acquired between June 15 and September 15. To be considered for analysis tree stems must be visible in the historic imagery allowing us to distinguish forest and shrub cover from herbaceous and unvegetated areas. We used the photo extents from the metadata to ensure that photos also overlapped with the available high-spatial-resolution satellite imagery for change comparison.

We selected 27 photos along four transects (15–70 km in length). Photos from Transect 2 (GSU) and Transect 3 (Whitefish West) were acquired in the 1930’s (1930 and 1937, respectively) and photos for Transect 1 (Coppermine) and Transect 4 (Whitefish East) were acquired in the ~ 1970’s (1969 and 1971, respectively). Air photos were georeferenced in ArcGIS Pro version 3.4.3 against the high-resolution satellite base map derived from pansharpened WorldView-2 and WorldView-3 imagery at 0.4 or 0.5 m spatial resolution, respectively. These basemaps are compiled by ESRI and combine multiple sources of satellite and aerial imagery providing < 1 m spatial resolution data for most of the world. For each transect we extracted metadata for the imagery including data source, date of acquisition and spatial resolution. To align the air photos to the satellite basemap, the ‘‘projective’’ image transformation type was used with a minimum of 15 control points. The size, scale and relative georeferencing error of the air photos varied by transect (Table 2). The average georeferencing error between the high-resolution datasets is expected to be less than half the width of a Landsat pixel (15 m). In comparison, following digitization the pixel size of the georeferenced air photos ranged from 0.2 to 0.3 m (Table 2).

Landsat Structural Vegetation Change

We assessed the agreement of vegetation change from high-resolution image interpretation with a model of vegetation structure derived from Landsat time-series and spaceborne lidar data from ICESat-2 (Travers-Smith and others, 2024, 2025). Vegetation structure was modeled using ICESat-2 observations to predict vegetation presence and 98th percentile height using a suite of spectral and topographic indices at 30 m spatial resolution (Travers-Smith and others 2024). The Landsat structural change layer (hereafter referred as LSC) classified change in these modeled attributes over six time periods between 1985 and 2022 (Table 3). Change classification is based on transitions between forest (> 3 m height), tall shrub (< 3 m height) and no canopy (probability of canopy presence < 50%) classes over time. As ICESat-2 does not reliably detect vegetation < 1 m in height, the shrub class represents tall shrubs and small trees generally between 1 and 3 m. Here we simplified the original nine classes into the following six: stable no canopy, stable tall shrub, stable forest, increasing forest structure, increasing tall shrub and decreasing structure (Table 3). The ‘‘increasing forest structure’’ class represents pixels with significant increasing trends in height and a median height over 3 m across the time series (Table 3). The ‘‘increasing tall-shrub structure’’ class represents pixels that transitioned from the no canopy class to the shrub (< 3 m) class (Table 3).

Table 2. Air Photo Characteristics and Metadata Across Transects Crossing the Historic Forest Limit

Transect	Air photo scale	Air photo dates	Total photo area	Average georeference RMSE	High-resolution satellite image dates	Air photo pixel size
Transect 1 (Coppermine) (n = 5)	1:15,000	09-04-1969	99.4 km^2	5.0 m	06-01-2024	0.25 m
Transect 2 (GSU) (n = 8)	1:20,000	09-07-1937	71.94 km^2	3.29 m	06–27–2019	0.30 m
Transect 3 (Whitefish West (n = 6)	1:12,000	07–25–1930	23.06 km^2	7.22 m	07–11–2022/07–23–2024	0.20 m
Transect 4: Whitefish East (n = 8)	1:20,000	07–29–1971	45.7 km^2	8.3 m	10-09-2023	0.30 m

Table 3. Descriptions of the Nine Landsat-Derived Structural Vegetation Types Classified At 30 m Spatial Resolution

Vegetation classes	Decision rules	Simplified classes
Stable no canopy	Majority no canopy class	Stable no canopy
Stable shrub (1–3 m)	Majority shrub class	Stable shrub
Stable forest (> 3 m)	Majority forest class & no trend in height	Stable forest
Stable low forest	Multiple transitions between forest and shrub but no trend in height	Stable forest
Forest growth	Majority forest class & significant increasing height	Increasing forest structure
New forest	Change from no canopy or shrub to forest	Increasing forest structure
New shrub	Change from no canopy to shrub	Increasing shrub structure
Forest to shrub transition	Forest to shrub change OR majority forest with decreasing height	Decreasing structure
Canopy loss	Change from forest or shrub to no canopy	Decreasing structure

Decision rules describe logic used to classify change in canopy presence and height across six time periods. The simplified classes used in this study are shown in the last column.

LSC data were projected and spatially aligned with the 300 × 300 m grid cells used in air photo image interpretation.

Data Analysis

Estimating Historic Land Cover with Photo Interpretation

We used the aerial photos to estimate historic percent cover for the following five land cover types: forest, shrubs, herbaceous vegetation (including graminoids, forbs, mosses, lichen), barren and water (Figure 2). We overlaid each air photo with a 300 × 300 m grid (n = 2063) encompassing the extent of the air photos (240 km^2) and visually estimated the percent cover of land cover within each cell using texture, shape and contrast cues. The cell size helps accommodate georeferencing error between the Landsat imagery and high-resolution photographs, while still capturing local patterns in vegetation change. Percent cover was estimated using following ranges: very low (1–5%), low (5–25%), moderate (25–40%), high (40–60%) and very high (> 60% cover). Due to the cell size used, we assumed the impact of georeferencing error (~ 3–9 m) between photos and satellite imagery was negligible. Images were viewed at multiple scales to identify vegetation and land cover types and to ensure mapping consistency across cells. Forests were identified based on the presence of trees which were distinguished by their conical shape and long shadows (Figure 2). The shrub class included both low and tall shrubs. Tall shrubs were identified based on their circular crowns and lack of shadows, while low shrubs were distinguished by their darker and textured appearance relative to lighter surrounding herbaceous land cover (Figure 2). Barren land cover was defined as unvegetated rock outcrops. Interpretation of land cover types was also aided by oblique aerial photography from nearby transects available from the NWT Ecosystem Classification Group (2013; photos available from the GWNT Centre for Geomatics: Geocortex Viewer for HTML5). A single interpreter was used to ensure mapping consistency across photos and transects.

Next, we compared historic air photos with pansharpened 2023–2024 satellite imagery and assessed change in percent cover within the same 300 × 300 m cells (Figure 2). For the high-resolution satellite imagery, shrubs were identified by their dark green color and contrast with surrounding herbaceous vegetation, rather than texture which was not clear in the imagery. All remaining herbaceous vegetation was grouped and identified based on its lighter color and homogeneous texture. Increasing and decreasing percent cover was assessed within the following ranges: no change, trace (1–5%), moderate (5–10%), high (10–20%) and very high (> 20%). The NWT Fire History dataset (NWT Centre for Geomatics, 2024) and the national Landsat product Composite2Change (Hermosilla and others, 2016) were used to identify stand replacing wildfires the burned between 1950 and 2022. The final photo interpretation dataset shows the historic proportion of land cover classes, the magnitude and direction

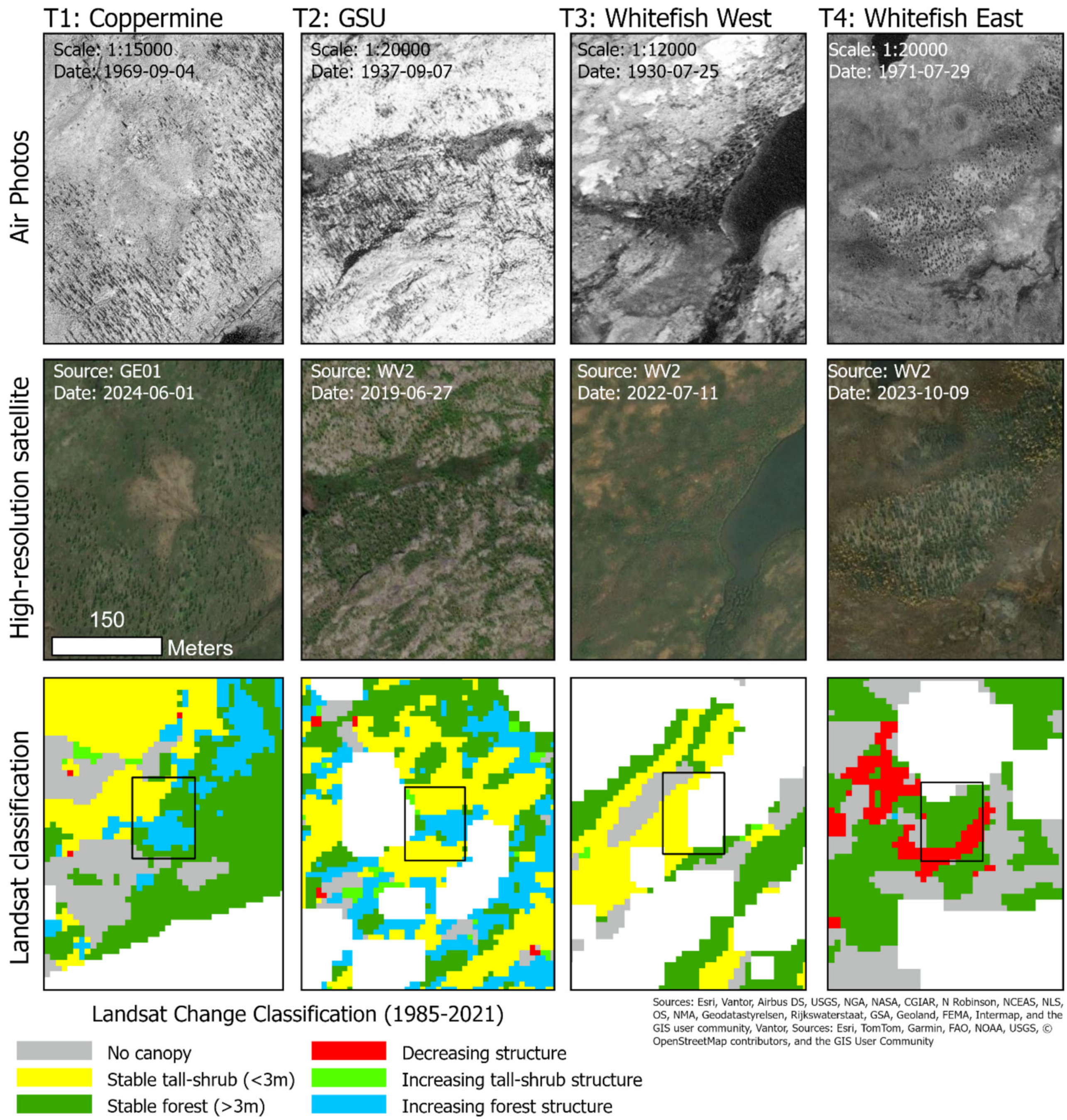

Figure 2. Examples of air photos and satellite imagery used to map change in forest and shrub cover across four transects crossing the forest-tundra ecotone. Dates are in year-month-day format. The bottom row shows the Landsat structural change classification maps at 30 m spatial resolution (Travers-Smith and others, 2025) and the black outline shows the extent of the fine-scale imagery within each transect. White areas are lakes and waterbodies that were removed from analysis. In the WorldView imagery from Transect 4, tamarack (*Larix Laricina*) is visible on the edges of the black spruce stand.

of change between historic air photos and high-resolution satellite images, and the fire history encompassing the extent of all air photos within 300 × 300 m cells.

Modeling Probability of Forest and Shrub Expansion

We used percent change in land cover from all 300 × 300 m cells to model the probability of increasing tree and shrub cover for each transect using a generalized linear mixed effect model. Distance to the treeline was a fit as a global fixed effect and random slopes and intercepts were used for each combination of vegetation type (forest or shrub) and transect. Change in tree and shrub cover was used as the response variable with a value of 0 for cells with no change or decreasing cover, or 1 for cells with increasing cover. A negative treeline distance indicates that the cell centerpoint was below the forest limit and a positive distance indicates that the centerpoint was above the forest limit. The model was fit using the R package lme4 with a binomial link function (Bates and others, 2015). To compare the effect of distance to treeline between sites and vegetation types, we reported the slope and intercept coefficients across levels and plotted the predicted probability of increasing vegetation cover against treeline distance within each transect.

Comparing Photo Interpretation with Landsat Time-Series

We compared the photo-interpreted change with the LSC layer within the 300 × 300 m grid cells and individual 30 m pixels (n = 646). In the 300 m grid cells, we compared the percent cover of herbaceous, shrub and forest estimated from the air photos to the proportion of the cell covered by corresponding stable LSC classes (no canopy, shrub, forest, respectively). To directly assess how change in tree and shrub cover was captured by Landsat classification we also sampled 646 individual 30 m pixels representing stable and increasing forest and shrub classes. For each transect, we randomly sampled up to 90 stable pixels, 60 increasing forest pixels and 30 increasing shrub pixels. These strata were proportional to the frequency of each class in the LSC data. The minimum distance between pixels was 60 m, and in cases where there were fewer than 30 pixels of specific class within a transect, all available pixels were chosen. In each sampled pixel, we examined the air photos and high-spatial-resolution satellite imagery and recorded whether there was increasing forest or shrub cover in the pixel. We used these data to test whether the Landsat time-series corresponds to fine-scale increases in tree and shrub cover identified using the air photos and high-spatial-resolution satellite imagery.

Results

Photo-Interpreted Change Across Transects

Change in vegetation cover was variable across transects and air photo acquisition dates (1970's and 1930's). Table 3 shows the proportion of 300 × 300 m grid cells exhibiting change in forest and shrub cover between the air photographs and the 2020's high-resolution satellite imagery. Forest cover was generally stable for Transect 1 (Coppermine) and Transect 2 (GSU), with 88% and 74% of cells showing no change in cover (Table 4). Transect 3 (Whitefish West) and Transect 4 (Whitefish East) showed a higher frequency of change with 43% and 65% of cells showing increasing forest cover, respectively. Across Transect 3. ''Data'' (Whitefish West), the majority (62%) of these increases were small (covering < 10% of the cell). In contrast, the magnitude of increasing forest cover at Transect 4 (Whitefish East) was more evenly distributed with a similar proportion of cells exhibiting trace (< 5%) and high (> 20%) increasing cover (Table 4; Figure 3). Notably, the increase in forest cover across Transect 4 (Whitefish East) appears driven by tamarack (*Larix laricina*) rather than black spruce (*Picea mariana)*, which was distinguished by its bright yellow crown in the early autumn satellite imagery (Figure 2). Transect 3 (Whitefish West) exhibited the highest rates of change in shrubs with 93% of cells showing some level of increasing shrub cover (Table 4). Shrub cover at Transect 1 (Coppermine) was the most stable with 78% of cells showing stability. Transect 2 (GSU) and Transect 4 (Whitefish East) had intermediate increases in shrub cover, with 44% and 58% showing increases, respectively.

Fires impacted 21% of all cells (n = 446). Transect 1 (Coppermine) had no disturbed cells and Transect 3 (Whitefish West) had the most, with 71% of all cells burned (Table 5). As expected, the proportion of cells with decreasing forest cover was greater in burned areas while unburned areas showed more increases in forest cover (Table 5). More recent fires (1994–2014) in Transect 3 (Whitefish East) and Transect 4 (Whitefish West) corresponded with increasing shrub cover in 90% and 82% of burned cells, respectively (Table 5). The older fires (1976, 1977) in Transect 2 (GSU) showed increasing forest and shrub cover in 13% and 28% of cells, respectively (Table 5). Despite a large fire in 2014 that covered 71% of Transect 3 (Whitefish West), forest cover was still greater in 2022 compared to 1930 for 38% of cells (Table 5).

Table 4. Percent of 300 m Grid Cells Showing Stability and Change in Forest and Shrub Cover Mapped Using Historic Air Photos and Modern High-Resolution Satellite Imagery

Forest Cover	Transect 1 Coppermine (1969)	Transect 2 GSU (1937)	Transect 3 Whitefish West (1930)	Transect 4 Whitefish East (1971)
No change %	88.8	74.4	39.2	16.9
Decreasing %	0.0	2.5	17.7	18.3
Trace increase (+ 1–5%)	8.0	16.4	27.2	18.7
Increase (5–10%)	2.9	5.4	12.0	18.8
Increase (10–20%)	0.2	1.2	3.8	17.0
Increase (> 20%)	0.0	0.2	0.0	10.2
Shrub Cover				
No change %	78.8	66.6	7.0	42.5
Decreasing %	0.2	0.0	0.0	0.6
Trace Increase (+ 1–5%)	8.5	21.2	22.2	17.8
Increase (5–10%)	7.8	8.4	39.2	19.5
Increase (10–20%)	3.9	3.2	27.2	12.2
Increase (> 20%)	0.7	0.5	4.4	7.5
Total grid cells	N = 411	N = 590	N = 158	N = 904

The likelihood of increasing forest and shrub cover also varied with distance to the forest limit (Figure 4). Forest cover was more likely to increase closer to the forest limit for every transect except Transect 1 (Coppermine), which showed a low probability of increasing forest cover across the entire ecotone (Figure 4). Similarly, shrub cover was also more likely to increase close to, or above the present forest limit, with significant increasing trends in Transect 1 (Coppermine) and Transect 2 (GSU) (Figure 4). Transect 3 (Whitefish West) and Trasect 4 (Whitefish East) showed less variation in the probability of shrub increase across the ecotone. The probability of increasing shrub cover was generally greater than forests, with the exception of Transect 4 (Whitefish East; Figure 4).

Agreement with Landsat Time-Series

The level of agreement in stable vegetation cover between the air photos and LSC layer within 300 × 300 m cells was also variable (Figure 5). Very low (1–5%) and low (5–25%) cover of stable herbaceous vegetation was generally not detected in the LSC data. Conversely, stable forest cover was greater in the LSC data, especially when forest cover was low (Figure 5). Stable shrub cover showed the least agreement between datasets. The percent cover of shrub in the LSC data was consistently lower compared to cover mapped using photo interpretation (Figure 5).

At the pixel-scale, the level of agreement between LSC classes and photo-interpreted change varied between the 1970's and 1930's photos and the vegetation type (Figure 6). Agreement between the LSC data and photo-interpreted change was highest for the stable classes, with 80% and 91% correlation for pixels classified as stable forest and shrub, respectively. Increases in forest cover were less frequent in the LSC data compared to the photo-interpreted dataset (Figure 6). Instances where the LSC data detected a change that was not identified in the photo record occurred in 12% of sampled pixels. However, 50% of pixels showed forest and shrub change in the photo interpretation dataset but not in the LSC data. The level of agreement also varied by vegetation type and photo year. The highest agreement was found for increasing forest cover using the 1970's photos, with 65% of pixels showing increases in both datasets. In the 1930's air photos only 44% of pixels with increasing forest cover were classified as such in the LSC data (Figure 6). Increases in shrub cover showed similar patterns, with LSC data matching 57% and 33% of photo-interpreted changes for the 1970's and 1930's photos, respectively (Figure 6).

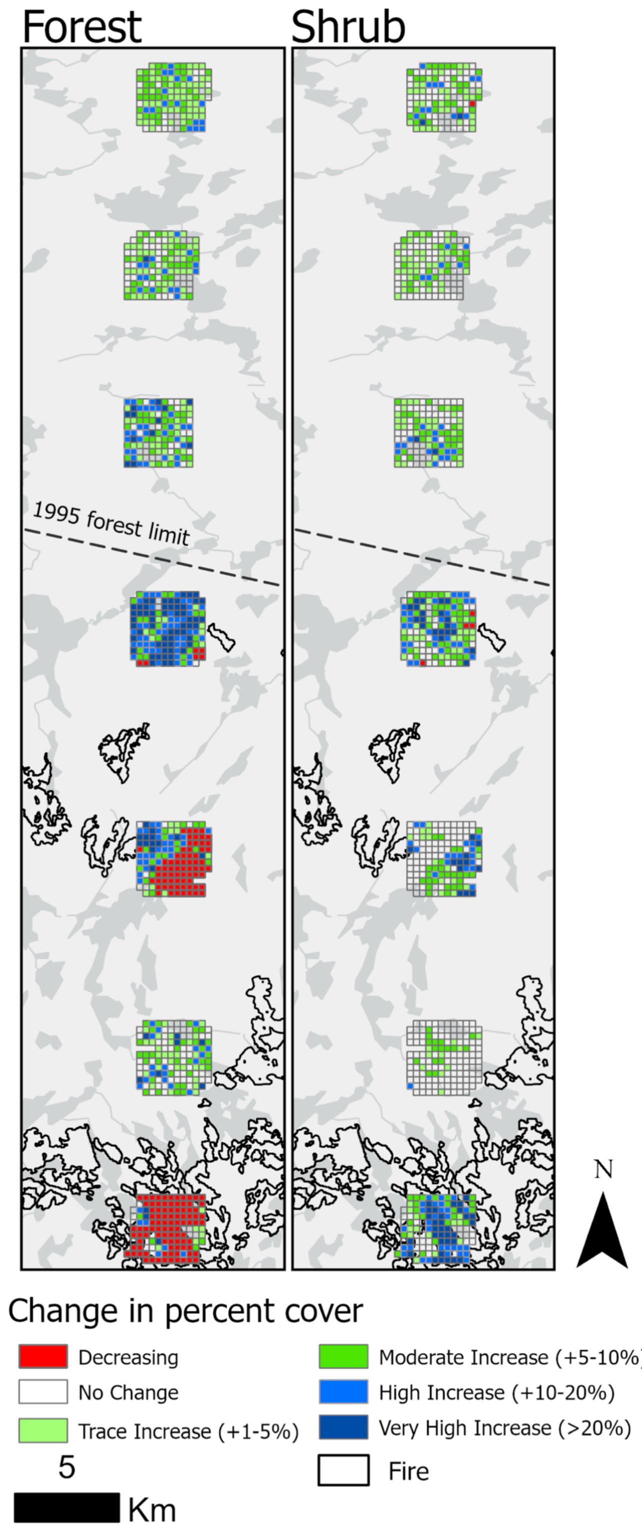

Figure 3. Change in forest and shrub cover for Transect 4 (Whitefish East) mapped in 300 m cells using the interpretation of historic air photos (1971) and high-spatial-resolution satellite imagery (2023).

Table 5. Summary of Fire History for Each Transect Showing the Proportion of 300 m Cells With Fire and the Year of the Fires Derived from the NWT Fire History and Composite2change Datasets

	Transect 1 (Coppermine) (1969)	Transect 2 (GSU) (1937)	Transect 3 (Whitefish West) (1930)	Transect 4 Whitefish East (1971)
% of burned cells				
Decreasing forest %	NA	6.1	23.7	83.9
Increasing forest %	NA	13.3	38.1	13.3
Increasing shrub %	NA	28.4	90.7	82.2
% of unburned cells				
Decreasing forest %	0.0	1.4	0.0	1.9
Increasing forest %	11.2	25.3	56.2	77.6
Increasing shrub %	20.9	35.1	97.9	50.7
% of total cells burned	0	25.1	71.1	20.0
Fire dates	NA	1976, 1977, 1994	2014	1994, 1997, 1998

Transect 1 (Coppermine) did not have any known fire. Percent change indicates the proportion of burned and unburned 300 m cells with increasing or decreasing forest and shrub cover.

Discussion

In this research, we used high-spatial-resolution air photos to map forest and shrub expansion across four forest-tundra transects in the NWT, Canada and compared these changes with Landsat time-series data. We showed that differences in fire history and regional climate influence the type and magnitude of change across transects. These dynamics were also broadly reflected in the satellite time-series data; however, varying performance highlights the need for careful interpretation and high-quality validation of modeled vegetation change. Overall, we found that shrub cover was more likely to increase compared to forests at three of the four sites. Forest cover was also more likely to increase closer to or above the historic forest limit at three of the four sites. Overall, fires and decreasing forest cover were common below the treeline, while forest expansion occurred in stands above the treeline where fire is less common and where trees can become established. Differences in forest and shrub expansion across sites were also likely driven by local factors such as fire history (Lantz and others, 2010; Walker and others, 2021), climate (Frost & Epstein, 2014; Lantz and others, 2019) and topography (Terskaia and others, 2020).

The southernmost sites hosting black spruce woodlands had greater increases in forest cover than the northernmost white spruce site, which could reflect warmer and wetter conditions at the southern sites. Correlation of forest and shrub expansion with Landsat-based change detection showed that forest change was better captured than shrub change. At the scale of individual pixels, Landsat change detection missed increases in forest and shrub cover that were detectable using high-resolution image interpretation. The level of agreement was also reduced when using the 1930’s photographs compared to the 1970’s photos, likely due to vegetation dynamics occurring between the 1930’s and the beginning of the satellite record (1985). Our analysis of multiple sites across the western Canadian forest-tundra ecotone highlights challenges in generalizing local patterns and the importance of validating vegetation change modeled using medium-resolution satellite data. Since we examined sites representative of the Taiga Shield our findings may not be applicable to forest-tundra sites outside of this region.

Climate and Fire History

Fire history was strongly related to vegetation dynamics at our southernmost black spruce sites,

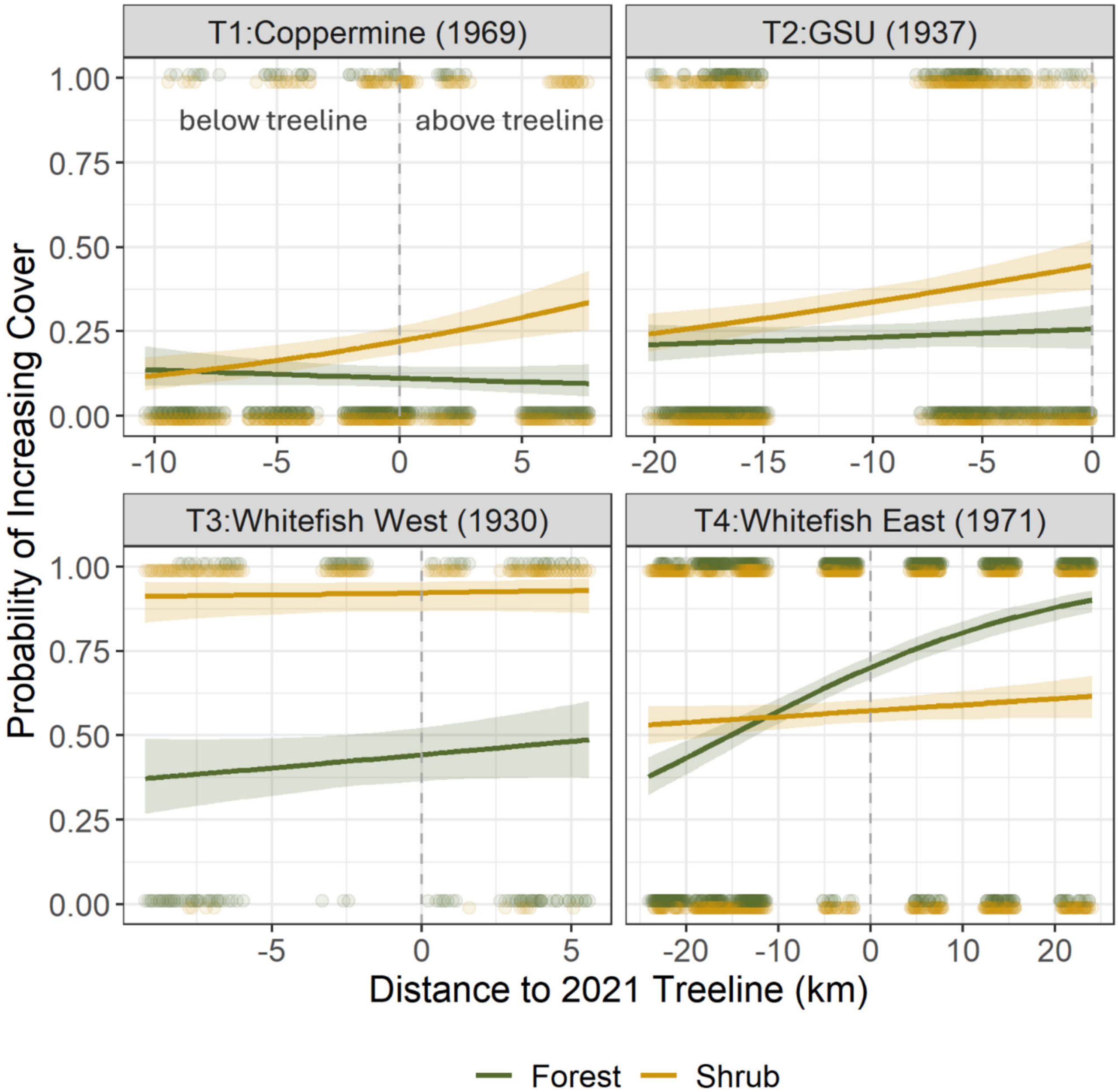

Figure 4. Probability that tree and shrub cover increased relative to the 2021 limit of continuous forest using all grid cells (n = 2063). The solid lines show the predicted probability for each combination of transect and vegetation type and the shaded area shows a 95% confidence interval of the prediction (Supplemental Table 1). Points represent individual grid cells and the gray-dashed line shows the position of the 2021 treeline.

driving large decreases in forest cover below the treeline. Smaller isolated woodlands above the treeline may be less likely to burn and tend to increase in area over time. This is consistent with national scale trends in treed area, where forest expansion was more likely to occur in northern compared to southern ecozones, and in proximity to existing treed areas (Hermosilla and others, 2025). Transect 4 (Whitefish East) also exhibited this trend, showing a strong increasing probability of forest cover expansion across the ecotone (Figure 3). This is also consistent with continental scale observations showing small increases in forest cover in the northern boreal, but large losses from fires in the southern part of the biome (Rotbarth and others, 2023; Timoney and others, 2019). Fires also likely drove increases in shrub cover (Lantz and others, 2010), with the 2014 fire in Transect 3 (Whitefish West) showing high (93%) rates of shrub expansion. Notably, at this site despite the

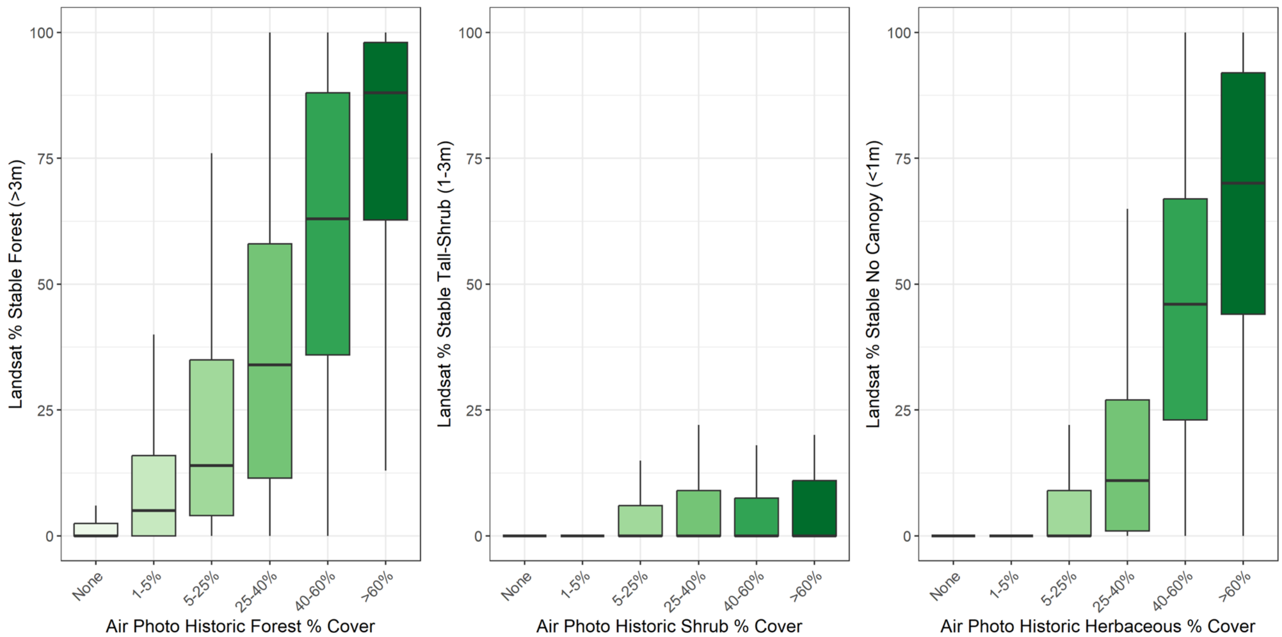

Figure 5. Boxplots showing correspondence between percent cover within 300 × 300 m cells for stable forest, shrub and herbaceous vegetation mapped on air photos and derived from Landsat time-series. Percent cover represents the proportion of the undisturbed cells where vegetation is present.

2014 fire, forest cover increased between 1930 and 2022 in 38% of cells. This could be a result of gradual forest infilling occurring over multiple decades, as well as lower intensity fire that left some trees intact.

Differences in climate may have also influenced patterns in forest and shrub expansion across our sites. Transect 1 (Coppermine) was the northernmost as well as coldest and driest site, with very little change in forested area of white spruce woodlands. In comparison, the three warmer sites closer to Yellowknife and Fort Reliance showed more frequent fires and a higher proportion of cells with forest expansion. Previous work suggests that precipitation and growing season length rather than air temperature may be stronger controls of forest and shrub expansion (Frost & Epstein, 2014; Maher and others, 2021). However, few long-term monitoring stations were available across our study region, challenging interpretation of precipitation trends at the regional scale. Pan-Arctic trends indicate that high latitudes are experiencing more precipitation overall, with a greater proportion falling as rain (McCrystall and others, 2021).

The width of the forest-tundra transition can also explain differences in forest advance observed across transects. Abrupt treelines occur when there is a strong environmental gradient that limits vegetation expansion, while diffuse treelines may experience less restrictions on seed availability and dispersion (Epstein and others, 2004; Montesano and others, 2020). Transect 1 (Coppermine) represents an abrupt transition between forest and non-forested tundra. Here we observed very little increase in forest cover above the historic forest limit compared to more diffuse transitions present at the other sites. In contrast, Transect 4: Whitefish East and the surrounding region host more isolated spruce stands above the forest limit (Timoney, 2023), which generally expanded in area over the observation period. Notably, this expansion appeared to be driven by tamarack (*Larix Laricina*), rather than black spruce. While it is unclear whether this is common at other treeline sites, labeled oblique air photos in the Whitefish Plain confirm mixed tamarack and black spruce stands are present at the treeline. Additionally, Baltzer and others, (2021) also note that post-fire tamarack regeneration occurs infrequently across boreal black spruce forests. While grayscale or pansharpened imagery can confirm the presence or absence of trees, color imagery acquired in the autumn from this area could be used to confirm species-specific tree expansion above the forest limit.

Landsat-Based Classification of Vegetation Change

The Landsat-based classification of vegetation change showed lower rates of forest and shrub

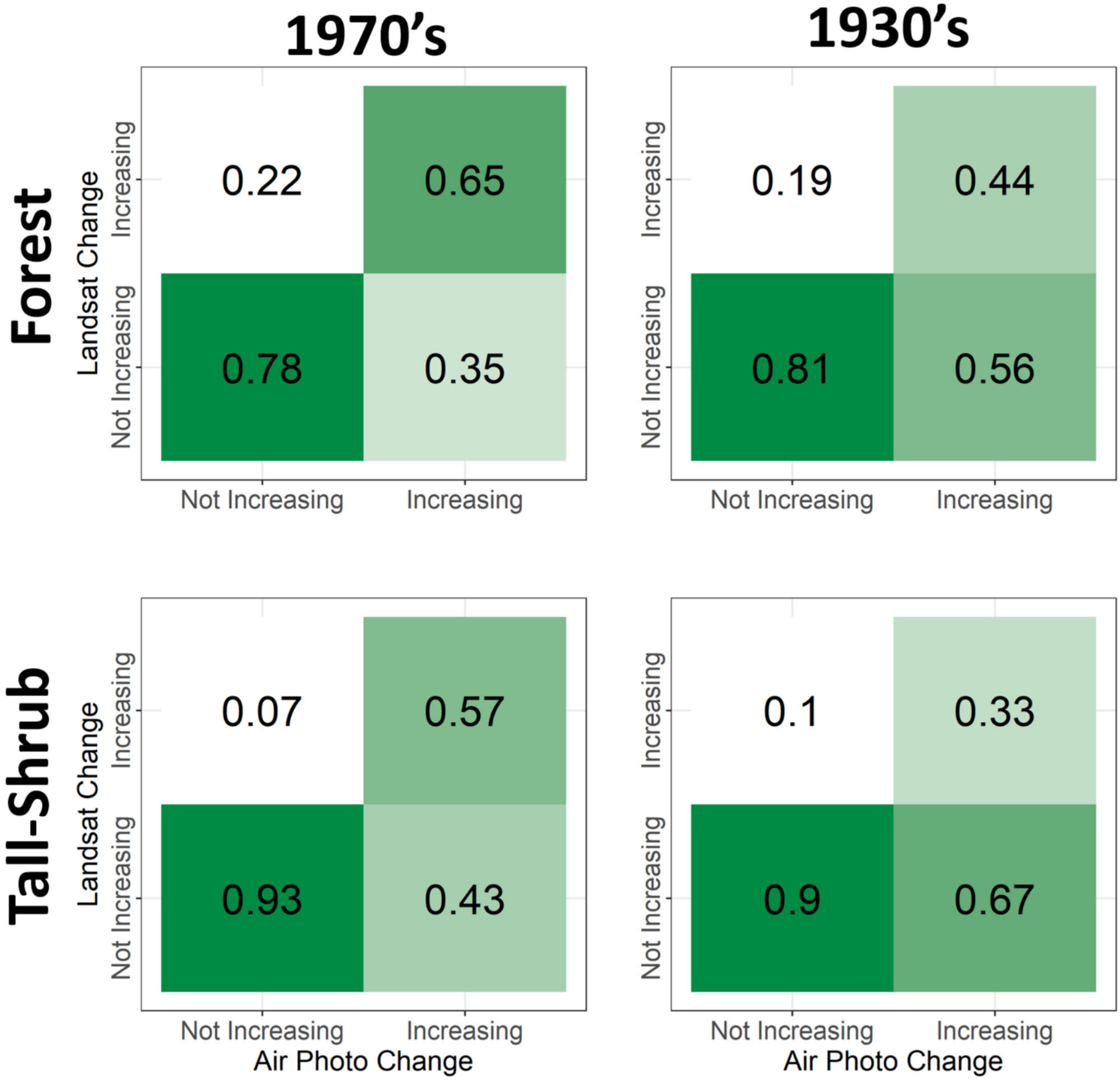

Figure 6. Co-occurrence matrices showing correspondence of vegetation change interpreted using high-resolution air photos (1970's and 1930's) and satellite imagery (2020's), with a Landsat time-series classification assessed in 30 m pixels (n = 646). The cell values show the proportion of pixels showing increasing or no change/decreasing cover in the Landsat time-series. The darker shades of green indicate higher correspondence.

expansion than image interpretation methods. Increasing vegetation structure was only detected in the Landsat classification 50% of the time across both time periods. However, agreement varied by vegetation type and the year of the air photo acquisition. Landsat change showed higher agreement with photo interpretation for 1970's transects compared to the 1930's which could reflect better image quality, or more likely, closer temporal alignment with the Landsat record starting in the 1980's. Change in vegetation cover that occurred between the 1930's and the beginning Landsat record would also reduce the correspondence in between datasets. Differences could also be because the lidar-informed remote sensing model is based on vertical structure while the photo interpretation methods detect horizontal cover. Additionally, at the scale of a single 30 m pixel, georeferencing error is expected to have a larger impact than the mapping conducted on a grid with 300 × 300 m cells. Spectral trends within the Landsat time-series is driven by factors other than tree and shrub change, including changes in understory composition (i.e., mosses and lichens), or soil and canopy moisture (Fraser and others, 2017; Myers-Smith and others, 2020). Previous validation of modeled tree cover at 30 m resolution in the forest-tundra shows greater uncertainty in open stands due to mixing with non-forested components, such as snow in the pixel (Hoad and others, 2025; Loranty and others, 2018).

Lower agreement between datasets for shrubs is likely due to uncertainty in mapping lower-stature vegetation in the LSC model and differences in how the shrub class was defined between data sources. The Landsat classification used ICESat-2 spaceborne lidar to model canopy height, where the shrub class is defined as vegetation 1–3 m in height, as low shrubs < 1 m are not consistently detectable with ICESat-2. However, in the photo interpretation data low and tall shrubs were not separated, resulting in much higher shrub cover in the interpretation dataset. Recent Landsat-based models using harvested biomass (Orndahl and others, 2025) and percent top-cover from drone imagery (Macander and others, 2022) may also be more sensitive to lower-stature tundra vegetation. Due to differences in modeling approach and training data, our specific Landsat change detection approach is not representative of all land cover or vegetation models for the forest-tundra in terms of accuracy or potential biases. However, the environmental covariates, modeling approach and validation of the Landsat-based approach are typical for this type of vegetation modeling (Coops and others, 2021; Hermosilla, Wulder, and others, 2022).

Limitations and Future Work

Our selection of historic air photos was opportunistic and restricted to transects that crossed the historic forest limit. Due to these restrictions, we were unable to acquire repeat aerial photography from the same sites, or within the Landsat satellite record (1985–present). To better understand rates of vegetation change over time, future work could compare spectral time-series to repeat aerial photography with multiple image dates coinciding with Landsat imagery, where possible. For example, Terskaia (2020) examined vegetation change across three image dates in Alaska. They found consistent shifts in vegetation type between earlier and later periods, suggesting that analysis of two image dates will still capture the majority of vegetation change. Our study was also limited by absence of ground-truth data to confirm photo interpretation results. However, labeled oblique aerial photographs taken as part of the NWT Ecosystem Classification (2008, 2009) greatly aided our interpretation.

Our initial search of the National Air Photo Library identified over 15,000 candidate photos within the Yukon, Northwest Territories and Nunavut from 1930 to 1999. This represents an information-rich dataset which could be used to validate and augment other remote sensing analyses across northern Canada using similar protocols (Hermosilla and others, 2022; Timoney & Mamet, 2020). By using photos across multiple sites and time periods, this study demonstrates the localized nature of vegetation change at the treeline and highlights opportunities to improve interpretation of models using medium-scale satellite remote sensing data.

Conclusions

In this paper we used historic air photos from the 1970's and 1930's and high-spatial-resolution satellite imagery to map change in forest and shrub cover across four sites in the Canadian forest-tundra ecotone. We observed variable patterns in forest and shrub expansion across the ecotone reflecting differences in climate, local fire history and existing forest cover. Our models suggest that the likelihood of forest and shrub expansion increases with proximity to the forest limit and increases in shrub density are closely linked to recent fire history. Increases in air temperature were similar over the study area but southern sites were generally warmer and are likely closer to change thresholds. We also compared photo-interpreted change with models of vegetation change derived from Landsat time-seriesmeasurements of canopy height from spaceborne lidar. Overall, the Landsat product was better at representing tall-stature forests and herbaceous vegetation. Shrub cover was underestimated as the lidar data did not consistently capture vegetation < 1 m in height. Higher agreement between air photo interpretation and Landsat-based models was observed for forest compared to shrub expansion, and for transects using the 1970's photos compared to older photos from the 1930's. This is likely due to greater overlap between the Landsat record (1985–2021) and the air photo acquisitions in the 1970's. These results show that Landsat time-series can capture regional differences in vegetation dynamics from 1985 to the present, but these dynamics should not be expected to be representative of conditions prior to

1985. This research also highlights the importance of high-spatial-resolution validation in remotely sensed models of vegetation change and the utility of Canadian National Air Photo Library in supporting these efforts.

ACKNOWLEDGEMENTS

This research was funded in part through the Canadian Space Agency (Grant number: 21SUESECDL). We also acknowledge funding support to Hana Travers-Smith from the NSERC Canada Graduate Scholarship-Doctoral and the University of British Columbia.

FUNDING

Natural Sciences and Engineering Research Council of Canada, Canada Graduate Scholarship, Canadian Space Agency, 21SUESECDL.

DATA AVAILABILITY

Datasets and code to reproduce the results and figures in this paper are available on GitHub at https://github.com/hztraver/Air-photo-mapping. Other publicly available datasets used in this study include: ICESat-2 ATL08 version 5 (https://nsidc.org/data/atl08/versions/5#anchor-2), ASTER Global Digital Elevation Model (https://lpdaac.usgs.gov/products/ast14demv003/). Landsat Best Available Pixel (BAP) Composites were generated from Landsat TM and ETM Level-1 Terrain-Corrected Surface Reflectance data (https://earthexplorer.usgs.gov/) and BAP composites used in this analysis are available on request from the authors. Air photos were acquired through the National Air Photo Library (https://www.eodms-sgdot.nrcan-rncan.gc.ca/index-en.html).

Declarations

Conflict of interest The authors declare the following financial interests/personal relationships which may be considered as potential competing interests: Hana Travers-Smith reports that financial support was provided by the Natural Sciences and Engineering Research Council of Canada. Nicholas Coops reports that financial support was provided by the Natural Sciences and Engineering Research Council of Canada.

REFERENCES

Baltzer JL, Day NJ, Walker XJ, Greene D, Mack MC, Alexander HD, Arseneault D, Barnes J, Bergeron Y, Boucher Y, Bourgeau-Chavez L, Brown CD, Carrière S, Howard BK, Gauthier S, Parisien M-A, Reid KA, Rogers BM, Roland C, Johnstone JF. 2021. Increasing fire and the decline of fire adapted black spruce in the boreal forest. Proceedings of the National Academy of Sciences 118(45):e2024872118. https://doi.org/10.1073/pnas.2024872118.

Bates D, Mächler M, Bolker B, Walker S. 2015. Fitting Linear Mixed-Effects Models Using lme4. Journal of Statistical Software 67(1):1–48. https://doi.org/10.18637/jss.v067.i01.

Beamish A, Raynolds MK, Epstein H, Frost GV, Macander MJ, Bergstedt H, Bartsch A, Kruse S, Miles V, Tanis CM, Heim B, Fuchs M, Chabrillat S, Shevtsova I, Verdonen M, Wagner J. 2020. Recent trends and remaining challenges for optical remote sensing of Arctic tundra vegetation: A review and outlook. Remote Sensing of Environment 246:111872. https://doi.org/10.1016/j.rse.2020.111872.

Beck PSA, Goetz SJ. 2011. Satellite observations of high northern latitude vegetation productivity changes between 1982 and 2008: Ecological variability and regional differences. Environmental Research Letters 6(4):045501. https://doi.org/10.1088/1748-9326/6/4/045501.

Berner, L. T., & Goetz, S. J. (2021). Satellite observations document trends consistent with a boreal forest biome shift. *Global Change Biology*, *28*. https://doi.org/10.1111/gcb.16121

Brandt, J. P. (2009). The extent of the North American boreal zone. *Environmental Reviews*, *17*(NA), 101–161. https://doi.org/10.1139/A09-004

Brodie JF, Roland CA, Stehn SE, Smirnova E. 2019. Variability in the expansion of trees and shrubs in boreal Alaska. Ecology 100(5):e02660. https://doi.org/10.1002/ecy.2660.

Coops NC, Tompalski P, Goodbody TRH, Queinnec M, Luther JE, Bolton DK, White JC, Wulder MA, van Lier OR, Hermosilla T. 2021. Modelling lidar-derived estimates of forest attributes over space and time: A review of approaches and future trends. Remote Sensing of Environment 260:112477. https://doi.org/10.1016/j.rse.2021.112477.

Cunliffe AM, Assmann JJ, Daskalova GN, Kerby JT, Myers-Smith IH. 2020. Aboveground biomass corresponds strongly with drone-derived canopy height but weakly with greenness (NDVI) in a shrub tundra landscape. Environmental Research Letters 15(12):125004. https://doi.org/10.1088/1748-9326/aba470.

Danby, R. K., & Hik, D. S. (2009). Evidence of Recent Treeline Dynamics in Southwest Yukon from Aerial Photographs. *ARCTIC*, *60*(4), 411–420. https://doi.org/10.14430/arctic198

Dial RJ, Maher CT, Hewitt RE, Sullivan PF. 2022. Sufficient conditions for rapid range expansion of a boreal conifer. Nature 608(7923):546–551. https://doi.org/10.1038/s41586-022-05093-2.

Dial RJ, Maher CT, Hewitt RE, Wockenfuss AM, Wong RE, Crawford DJ, Zietlow MG, Sullivan PF. 2024. Arctic sea ice retreat fuels boreal forest advance. Science 383(6685):877–884. https://doi.org/10.1126/science.adh2339.

Ecosystem Classification Group. (2008). *Ecological Regions of the Northwest Territories – Taiga Shield.* (p. viii + 146 pp. + insert map). Department of Environment and Natural Resources, Government of the Northwest Territories. https://www.enr.gov.nt.ca/sites/enr/files/resources/taiga_shield_ecological_land_classification_report_0.pdf

Epstein HE, Beringer J, Gould WA, Lloyd AH, Thompson CD, Chapin FS, Michaelson GJ, Ping CL, Rupp TS, Walker DA. 2004. The Nature of Spatial Transitions in the Arctic. Journal of Biogeography 31(12):1917–1933.

Feng, M., Sexton, J. O., Wang, P., Montesano, P. M., Calle, L., Carvalhais, N., Poulter, B., Macander, M. J., Wulder, M. A., Wooten, M., Wagner, W., Elders, A., Channan, S., & Neigh, C. S. R. (2025). Northward shift of boreal tree cover confirmed by satellite record. *EGUsphere*, 1–20. https://doi.org/10.5194/egusphere-2025-2268

Foster AC, Shuman JK, Rogers BM, Walker XJ, Mack MC, Bourgeau-Chavez LL, Veraverbeke S, Goetz SJ. 2022. Bottom-up drivers of future fire regimes in western boreal North America. Environmental Research Letters 17(2):025006. https://doi.org/10.1088/1748-9326/ac4c1e.

Fraser RH, Lantz TC, Olthof I, Kokelj SV, Sims RA. 2014. Warming-Induced Shrub Expansion and Lichen Decline in the Western Canadian Arctic. Ecosystems 17(7):1151–1168. https://doi.org/10.1007/s10021-014-9783-3.

Fraser, R. H., Van der Sluijs, J., & Hall, R. J. (2017). Calibrating Satellite-Based Indices of Burn Severity from UAV-Derived Metrics of a Burned Boreal Forest in NWT, Canada. *Remote Sensing*, *9*(3), Article 3. https://doi.org/10.3390/rs9030279

Frost GV, Epstein HE. 2014. Tall shrub and tree expansion in Siberian tundra ecotones since the 1960s. Global Change Biology 20(4):1264–1277. https://doi.org/10.1111/gcb.12406.

Frost, G. V., Bhatt, U. S., Macander, M. J., Berner, L. T., Walker, D. A., Raynolds, M. K., Magnússon, R. Í., Bartsch, A., Bjerke, J. W., Epstein, H. E., Forbes, B. C., Goetz, S. J., Hoy, E. E., Karlsen, S. R., Kumpula, T., Lantz, T. C., Lara, M. J., López-Blanco, E., Montesano, P. M., … Waigl, C. F. (2025). The changing face of the Arctic: Four decades of greening and implications for tundra ecosystems. *Frontiers in Environmental Science*, *13*, 1525574. https://doi.org/10.3389/fenvs.2025.1525574

Hermosilla T, Wulder MA, White JC, Coops NC, Hobart GW, Campbell LB. 2016. Mass data processing of time series Landsat imagery: Pixels to data products for forest monitoring. International Journal of Digital Earth 9(11):1035–1054. https://doi.org/10.1080/17538947.2016.1187673.

Hermosilla T, Wulder MA, White JC, Coops NC. 2022. Land cover classification in an era of big and open data: Optimizing localized implementation and training data selection to improve mapping outcomes. Remote Sensing of Environment 268:112780. https://doi.org/10.1016/j.rse.2021.112780.

Hermosilla, T., Wulder, M. A., White, J. C., Bater, C. W., Baral, S. K., & Leach, J. A. (2025). Expansion of treed area over Canada's forested ecosystems: Spatial and temporal trends. *Forestry: An International Journal of Forest Research*, *1*(14), cpaf015. https://doi.org/10.1093/forestry/cpaf015

Hoad CG, Myers-Smith IH, Kerby JT, Colesie C, Assmann JJ. 2025. Snow persistence lowers and delays peak NDVI, the vegetation index that underpins Arctic greening analyses. Environmental Research Letters 20(3):034019. https://doi.org/10.1088/1748-9326/adacff.

Lantz TC, Moffat ND, Fraser RH, Walker X. 2019. Reproductive limitation mediates the response of white spruce (*Picea glauca*) to climate warming across the forest–tundra ecotone. Arctic Science 5(4):167–184. https://doi.org/10.1139/as-2018-0012.

Lantz, T. C., Gergel, S. E., & Henry, G. H. R. (2010). Response of green alder (Alnus viridis subsp. Fruticosa) patch dynamics and plant community composition to fire and regional temperature in north-western Canada. *Journal of Biogeography*, *37*(8), 1597–1610. https://doi.org/10.1111/j.1365-2699.2010.02317.x

Loranty M, Davydov S, Kropp H, Alexander H, Mack M, Natali S, Zimov N. 2018. Vegetation Indices Do Not Capture Forest Cover Variation in Upland Siberian Larch Forests. Remote Sensing 10(11):1686. https://doi.org/10.3390/rs10111686.

Macander MJ, Nelson PR, Nawrocki T, Frost GV, Orndahl K, Palm EC, Wells AF, Goetz SJ. 2022. Time-series maps reveal widespread change in plant functional type cover across arctic and boreal Alaska and Yukon. Environmental Research Letters. https://doi.org/10.1088/1748-9326/ac6965.

Maher CT, Dial RJ, Pastick NJ, Hewitt RE, Jorgenson MT, Sullivan PF. 2021. The climate envelope of Alaska's northern treelines: Implications for controlling factors and future treeline advance. Ecography 44(11):1710–1722. https://doi.org/10.1111/ecog.05597.

McCrystall, M. R., Stroeve, J., Serreze, M., Forbes, B. C., & Screen, J. A. (2021). New climate models reveal faster and larger increases in Arctic precipitation than previously projected. *Nature Communications*, *12*(1), Article 1. https://doi.org/10.1038/s41467-021-27031-y

Mekonnen ZA, Grant RF, Schwalm C. 2018. Modelling impacts of recent warming on seasonal carbon exchange in higher latitudes of North America. Arctic Science 4(4):471–484. https://doi.org/10.1139/as-2016-0009.

Moffat ND, Lantz TC, Fraser RH, Olthof I. 2016. Recent Vegetation Change (1980–2013) in the Tundra Ecosystems of the Tuktoyaktuk Coastlands, NWT, Canada. Arctic, Antarctic, and Alpine Research 48(3):581–597. https://doi.org/10.1657/AAAR0015-063.

Montesano PM, Nelson R, Sun G, Margolis H, Kerber A, Ranson KJ. 2009. MODIS tree cover validation for the circumpolar taiga–tundra transition zone. Remote Sensing of Environment 113(10):2130–2141. https://doi.org/10.1016/j.rse.2009.05.021.

Montesano PM, Neigh CSR, Macander M, Feng M, Noojipady P. 2020. The bioclimatic extent and pattern of the cold edge of the boreal forest: The circumpolar taiga-tundra ecotone. Environmental Research Letters 15(10):105019. https://doi.org/10.1088/1748-9326/abb2c7.

Myers-Smith, I. H., Kerby, J. T., Phoenix, G. K., Bjerke, J. W., Epstein, H. E., Assmann, J. J., John, C., Andreu-Hayles, L., Angers-Blondin, S., Beck, P. S. A., Berner, L. T., Bhatt, U. S., Bjorkman, A. D., Blok, D., Bryn, A., Christiansen, C. T., Cornelissen, J. H. C., Cunliffe, A. M., Elmendorf, S. C., … Wipf, S. (2020). Complexity revealed in the greening of the Arctic. *Nature Climate Change*, *10*(2), Article 2. https://doi.org/10.1038/s41558-019-0688-1

Natural Resources Canada. (2011, June 14). *National Air Photo Library*. https://natural-resources.canada.ca/maps-tools-publications/satellite-elevation-air-photos/air-photos-library/national-air-photo-library

NWT Centre for Geomatics. (2024). *Fire History* . https://www.geomatics.gov.nt.ca/en/fire-history

Olofsson P, Foody GM, Herold M, Stehman SV, Woodcock CE, Wulder MA. 2014. Good practices for estimating area and assessing accuracy of land change. Remote Sensing of Environment 148:42–57. https://doi.org/10.1016/j.rse.2014.02.015.

Orndahl KM, Macander MJ, Berner LT, Goetz S. 2022. Plant functional type aboveground biomass change within Alaska and northwest Canada mapped using a 35-year satellite time series from 1985–2020. Environmental Research Letters. https://doi.org/10.1088/1748-9326/ac9d50.

Orndahl, K. M., Berner, L. T., Macander, M. J., Arndal, M. F., Alexander, H. D., Humphreys, E. R., Loranty, M. M., Ludwig, S. M., Nyman, J., Juutinen, S., Aurela, M., Mikola, J., Mack,

M. C., Rose, M., Vankoughnett, M. R., Iversen, C. M., Kumar, J., Salmon, V. G., Yang, D., … Goetz, S. J. (2025). Next generation Arctic vegetation maps: Aboveground plant biomass and woody dominance mapped at 30 m resolution across the tundra biome. *Remote Sensing of Environment*, *323*, 114717. https://doi.org/10.1016/j.rse.2025.114717

Payette, S., Fortin, M.-J., & Gamache, I. (2001). The Subarctic Forest–Tundra: The Structure of a Biome in a Changing Climate: The shifting of local subarctic tree lines throughout the forest–tundra biome, which is linked to ecological processes at different spatiotemporal scales, will reflect future global changes in climate. *BioScience*, *51*(9), 709–718. https://doi.org/10.1641/0006-3568(2001)051%255B0709:TSFTTS%255D2.0.CO;2

Rickbeil GJM, Hermosilla T, Coops NC, White JC, Wulder MA, Lantz TC. 2018. Changing northern vegetation conditions are influencing barren ground caribou (Rangifer tarandus groenlandicus) post-calving movement rates. Journal of Biogeography 45(3):702–712. https://doi.org/10.1111/jbi.13161.

Rotbarth R, Van Nes EH, Scheffer M, Jepsen JU, Vindstad OPL, Xu C, Holmgren M. 2023. Northern expansion is not compensating for southern declines in North American boreal forests. Nature Communications 14(1):3373. https://doi.org/10.1038/s41467-023-39092-2.

Terskaia A, Dial RJ, Sullivan PF. 2020. Pathways of tundra encroachment by trees and tall shrubs in the western Brooks Range of Alaska. Ecography 43(5):769–778. https://doi.org/10.1111/ecog.05015.

Timoney KP. 2023. No evidence of a northward biome shift of treeline in the Mackay Lake region, north-central Canada. Écoscience 30(2):113–129. https://doi.org/10.1080/11956860.2023.2231262.

Timoney KP, Mamet S. 2020. No treeline advance over the last 50 years in subarctic western and central Canada and the problem of vegetation misclassification in remotely sensed data. Écoscience 27(2):93–106. https://doi.org/10.1080/11956860.2019.1698258.

Timoney KP, Mamet SD, Cheng R, Lee P, Robinson AL, Downing D, Wein RW. 2019. Tree cover response to climate change in the forest-tundra of north-central Canada: Fire-driven decline, not northward advance. Écoscience 26(2):133–148. https://doi.org/10.1080/11956860.2018.1532868.

Timoney, K. P., La Roi, G. H., Zoltai, S. C., & Robinson, A. L. (1992). The High Subarctic Forest-Tundra of Northwestern Canada: Position, Width, and Vegetation Gradients in Relation to Climate. *ARCTIC*, *45*(1), 1–9. https://doi.org/10.14430/arctic1367

Travers-Smith, H., Coops, N., Mulverhill, C., Wulder, M. A., Lantz, T. C., & Ignace, D. (2025). Satellite observations reveal stable forest limits and shrub expansion across the Canadian forest-tundra ecotone. *Environmental Research Letters*, *20*(10). https://doi.org/10.1088/1748-9326/adfc7f

Travers-Smith HZ, Lantz TC. 2020. Leading-edge disequilibrium in alder and spruce populations across the forest–tundra ecotone. Ecosphere 11(7):e03118. https://doi.org/10.1002/ecs2.3118.

Walker XJ, Howard BK, Jean M, Johnstone JF, Roland C, Rogers BM, Schuur EAG, Solvik KK, Mack MC. 2021. Impacts of pre-fire conifer density and wildfire severity on ecosystem structure and function at the forest-tundra ecotone. PLOS ONE 16(10):e0258558. https://doi.org/10.1371/journal.pone.0258558.

Wulder, M. A., Roy, D. P., Radeloff, V. C., Loveland, T. R., Anderson, M. C., Johnson, D. M., Healey, S., Zhu, Z., Scambos, T. A., Pahlevan, N., Hansen, M., Gorelick, N., Crawford, C. J., Masek, J. G., Hermosilla, T., White, J. C., Belward, A. S., Schaaf, C., Woodcock, C. E., … Cook, B. D. (2022). Fifty years of Landsat science and impacts. *Remote Sensing of Environment*, *280*, 113195. https://doi.org/10.1016/j.rse.2022.113195